Synchronization of polarization chaos in mutually coupled free-running VCSELs

Wang, Ziruo; Li, Pu; Jia, Zhiwei; Wang, Wenjie; Xu, Bingjie; Shore, K. Alan; Wang, Yuncai

Opt. Express

DOI:
10.1364/OE.425674

Published: 01/06/2021

Publisher's PDF, also known as Version of record

Research Article | Vol. 29, No. 12 / 7 June 2021 / Optics Express 17940
Optics EXPRESS

Synchronization of polarization chaos in mutually coupled free-running VCSELs

ZIRUO WANG,[1] PU LI,[1,2,*] ZHIWEI JIA,[1] WENJIE WANG,[1] BINGJIE XU,[3] K. ALAN SHORE,[4] AND YUNCAI WANG[2,5]

[1]*Key Laboratory of Advanced Transducers and Intelligent Control System, Ministry of Education and Shanxi Province, Taiyuan University of Technology, Taiyuan 030024, China*
[2]*School of Information Engineering, Guangdong University of Technology, Guangzhou 510006, China*
[3]*Science and Technology on Communication Security Laboratory, Institute of Southwestern Communication, Chengdu 610041, China*
[4]*School of Electronic Engineering, Bangor University, Wales LL57 1UT, UK*
[5]*Guangdong Provincial Key Laboratory of Photonics Information Technology, Guangzhou 510006, China*
[*]*lipu8603@126.com*

Abstract: We numerically demonstrate and analyze polarization chaos synchronization between two free-running vertical cavity surface emitting semiconductor lasers (VCSELs) in the mutual coupling configuration under two scenarios: parallel injection and orthogonal injection. Specifically, we investigate the effect of external parameters (the bias current, frequency detuning and coupling coefficient) and internal parameters (the linewidth enhancement factor, spin-flip relaxation rate, field decay rate, carrier decay rate, birefringence and dichroism) on the synchronization quality. Finally simulation results confirm that in the parallel injection, chaotic synchronization can reach a cross-correlation coefficient of 0.99 within a range of parameter mismatch ±12%. On the other hand, the chaos synchronization for orthogonal injection only reaches a cross-correlation coefficient of 0.95 within a range of parameter mismatch ±3%.

1. Introduction

Laser chaos synchronization has received extensive attention due to its advantage in securing the physical layer of optical communication systems [1,2]. Unlike electric chaos, the high-bandwidth of the laser chaos has driven transmission rate of the chaos synchronization based communication to the level of 10 Gb/s with a low bit error rate [3–8]. Besides, some secure key distribution techniques based on chaos synchronization in optics have been proposed and considered as an attractive candidate from the point of view of practical feasibility in recent years [9,10].

There have been numerous studies on laser chaos synchronization where semiconductor lasers are the most widely used optical sources for generating chaotic light. For instance, Li et al. theoretically analyzed the generalized chaos synchronization in an open-loop unidirectionally coupled configuration where both the transmitter and the receiver are single-longitudinal-mode semiconductor lasers [11]. Jiang *et al*. systematically investigated the properties of injection-locking chaos synchronization and communication in closed-loop external-cavity semiconductor lasers subject to phase-conjugate feedback [12]. Hong *et al*. experimentally achieved chaos synchronization in two unidirectionally coupled vertical cavity surface emitting semiconductor lasers (VCSELs) with external feedback [13]. The implementation of chaos communication using VCSELs motivates further investigations on the influence of polarization dynamics such as polarization maintaining, polarization rotation and polarization mode competition on the synchronization properties [14–16]. Englert *et al*. experimentally demonstrated zero-lag synchronization in a mutually coupled chaotic semiconductor laser system [17]. Xiang *et al*. numerically investigated the chaos synchronization properties in a hierarchical tree-type optical

#425674 https://doi.org/10.1364/OE.425674
Journal © 2021 Received 22 Mar 2021; revised 30 Apr 2021; accepted 17 May 2021; published 25 May 2021

Optics EXPRESS

network consisting of mutually coupled semiconductor lasers (SLs) [18]. Li *et al*. studied the optical chaos synchronization in point-to-multipoint (PTM) and ring networks [19].

However, it should be pointed out that most semiconductor lasers used for the aforementioned chaotic communication systems can not directly output chaotic signals, but commonly require an external perturbation such as time-delayed optical feedback to be driven into chaos. As such the arrangements are relatively complex to setup, run and maintain. To guarantee a good synchronization property, much effort has to be devoted to the control of the chaotic dynamics [20].

It has previously been demonstrated that a solitary VCSEL under certain conditions can directly generate chaotic light without the need of additional external optical feedback, namely as polarization chaos [21]. This approach is much simpler and compact, which meets the current needs of integrating lasers into complex optical systems [22], and thus may significantly change the current scenario of chaotic communication systems. In 2016, Virte *et al*. demonstrated the unidirectional coupling injection locking synchronization of polarization chaos using two free-running VCSELs [23].

In this paper, we theoretically investigate the mutually coupled synchronization characteristics of polarization chaos. Specific investigations are executed in two scenarios where two chaotic VCSELs are subjected to parallel injection and orthogonal injection, respectively. We analyze the effect of bias current, coupling coefficient and frequency detuning between the mutually injected VCSELs in detail. Furthermore we examine the robustness of the mutually coupled chaotic synchronization under some mismatch of internal parameters (i.e., the line width enhancement factor, spin inversion relaxation rate, field attenuation rate, carrier attenuation rate, birefringence and dichroism). Finally simulation results demonstrate that the maximum cross-correlation coefficient in the case of parallel injection can reach 0.99 with a tolerable parameter mismatch range of ±12%. On the other hand, the correlation value of orthogonal injection can reaches 0.95 only when the coupling coefficient increases to 200~400 ns^{-1} with a relatively small tolerable parameter mismatch range of ±3%. Those two injection methods stimulate different dynamic mechanisms, which may be used in multi-channel optical communication systems [24].

2. Theory

Figure 1 shows the schematic for polarization chaos synchronization in two mutually coupled free running VCSELs. Both the VCSELs operate in the chaotic state without additional external perturbation. Specific investigations on the polarization chaos synchronization are executed in two cases: parallel optical injection and orthogonal optical injection. In the configuration of parallel optical injection [Fig. 1(a)], the laser output from VCSEL1 is connected to a polarization beam splitter (PBS1) to select the parallel (X) and vertical (Y) polarizations. Then, the X and Y linearly polarized lights attenuated by their own neutral density filters (NDFs) are injected into VCSEL2 via another polarization beam splitter (PBS2). This guarantees that the linear polarization directions of the injected light from VCSEL1 and the other VCSEL (VCSEL2) are parallel, and vice versa. As for the case of orthogonal optical injection [Fig. 1(b)], the X and Y linearly polarized lights from VCSEL1 is injected orthogonally to the Y and X linear polarization of VCSEL2, respectively. Note, the symbols M1, M2, M3 and M4 in Fig. 1 denote mirrors.

In our simulation, we use the well-known spin flip model (SFM) to describe the polarization chaos dynamics of the free-running VCSEL lasers [25–27]. The associated rate equations can be expressed as follows, where the second row in Eqs. (1) and (2) represent the coupling terms between X and Y polarization in the mutually injected configurations, respectively.

$$\begin{aligned}\frac{dE_x^{1,2}}{dt} &= \kappa^{1,2}(1+i\alpha^{1,2})[(N^{1,2}-1)E_x^{1,2}+in^{1,2}E_y^{1,2}]-(\gamma_\alpha^{1,2}+i\gamma_p^{1,2})E_x^{1,2}\\ &\quad + k_{inj_x}^{2,1}E_x^{2,1}(t-\tau_c)e^{-i\omega_0^{2,1}\tau_c}\mp i\Delta\omega E_x^{1,2}\end{aligned} \tag{1}$$

Optics EXPRESS

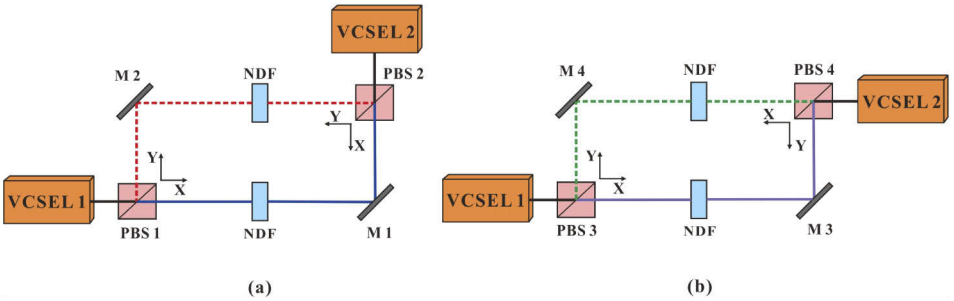

Fig. 1. Schematic for polarization chaos synchronization in two mutually coupled/injected VCSELs in two cases of (a) parallel optical injection and (b) orthogonal optical injection. PBS1, PBS2, PBS3, and PBS4, polarizing beam splitters; NDF, neutral density filter; M1, M2, M3 and M4, mirrors.

$$\begin{aligned}\frac{dE_y^{1,2}}{dt} &= \kappa^{1,2}(1+i\alpha^{1,2})[(N^{1,2}-1)E_y^{1,2} - in^{1,2}E_x^{1,2}] + (\gamma_\alpha^{1,2} + i\gamma_p^{1,2})E_y^{1,2} \\ &\quad + k_{inj_y}^{2,1}E_y^{2,1}(t-\tau_c)e^{-i\omega_0^{2,1}\tau_c} \mp i\Delta\omega E_y^{1,2}\end{aligned} \tag{2}$$

$$\frac{dN^{1,2}}{dt} = -\gamma_N{}^{1,2}[N^{1,2}(1+|E_x^{1,2}|^2+|E_y^{1,2}|^2) - \mu^{1,2} + in^{1,2}(E_y^{1,2}E_x^{*1,2} - E_x^{1,2}E_y^{*1,2})] \tag{3}$$

$$\frac{dn^{1,2}}{dt} = -\gamma_s^{1,2}n^{1,2} - \gamma_N^{1,2}[n^{1,2}(|E_x^{1,2}|^2+|E_y^{1,2}|^2) + iN^{1,2}(E_y^{1,2}E_x^{*1,2} - E_x^{1,2}E_y^{*}E_y^{*1,2})]. \tag{4}$$

Herein, E_x and E_y are the slowly varying electrical fields for the X and Y polarization. $N^{1,2}$ is the total carrier population, while $n^{1,2}$ is the carrier population difference. Note, the subscripts x and y stand for the X and Y polarizations, while the superscripts 1 and 2 represent VCSEL1 and VCSEL2, respectively. Equations (1) and (2) represent the expressions of the X and Y polarization change fields during parallel injection. For the case of orthogonal, $k_{inj\ x}$ and E_x in the second line of Eq. (1) should replaced into $k_{inj\ y}$ and E_y, while $k_{inj\ y}$ and E_y in the second line of Eq. (2) should be replaced into $k_{inj\ x}$ and E_x. The used internal parameters in the model are the field decay rate $\kappa = 600\ \text{ns}^{-1}$, the linewidth enhancement factor $\alpha = 3$, the carrier decay rate $\gamma_N = 1\ \text{ns}^{-1}$, the spin-flip relaxation rate $\gamma_s = 50\ \text{ns}^{-1}$, the birefringence $\gamma_p = 30\ \text{ns}^{-1}$, and the dichroism $\gamma_a = -0.7\ \text{ns}^{-1}$, respectively. The other external parameters $\Delta\omega$=2πΔf and k_{inj} denote the detuning and the coupling coefficient between VCSEL1 and VCSEL2, while the bias current μ varies. Note, in our simulation, Δf is the optical frequency detuing which varies from −40 to 40 GHz. It is well-appreciated [28] that the time of flight coupling time between the lasers should be taken into account in evaluating synchronization quality. For simplicity, in the present case we consider back to back coupling of the VCSELs so that the coupling time may be set to zero.

Finally, we introduce the correlation coefficient $C(\tau)$ defined as a function of the time delay τ to evaluate the polarization chaos synchronization quality as follows.

$$C(\tau) = \frac{\langle A(t)B(t+\tau)\rangle}{\sqrt{\langle A^2\rangle\langle B^2\rangle}} \tag{5}$$

Herein, $A(t) = a(t)$ - $<a(t)>$ and $B(t) = b(t)$ - $<b(t)>$ with $<\bullet>$ as the time average are defined for the time series a(t) and b(t) from VCSEL1 and VCSEL 2.

Furthermore, we use the synchronization error σ_{error} to characterize the effect of parameter mismatch on the robustness of the polarization chaos synchronization. Specifically, the

Optics EXPRESS

synchronization error σ_{error} is defined as follows.

$$\sigma_{\text{error}} = \frac{\langle |a(t) - b(t)| \rangle}{\langle b(t) \rangle} \tag{6}$$

where |•| is the absolute value symbol and <•> is the average value symbol. To meet the requirements of information transmission, the synchronization error σ_{error} should be controlled below 10% [29].

3. Simulation results and analysis

3.1. P-I curve and bifurcation diagram of the free-running VCSEL

Before investigating polarization chaos synchronization, we analyze the P-I characteristics of the free-running VCSELs and ensure both *X* and *Y* polarization modes in VCSELs are chaotic. Figure 2(a) shows the polarization-resolved P-I curve of the free-running VCSEL. As is apparent, the *X* polarization mode begins to oscillate when the bias current μ is at the threshold (I_{th}) and then increases linearly. On the other hand, the *Y* polarization mode cannot be observed until $\mu = 3.2$. In the range of $3.2 < \mu < 5$, the *X* and *Y* polarization modes exist simultaneously. Figures 2(b) and 2(c) illustrates the bifurcation diagram of the local extremes of the intensity time series of the *X* and *Y* polarization mode as a function of the normalized bias current, respectively. From it, we can determine that with increase of μ, the VCSEL undergoes a transition from periodic output into a chaotic regime. In the range of 3.8< μ <4.7 and 5.2following simulations < μ <6, both *X* and *Y* polarization modes will chaotically oscillate at the same time. Finally, we set the bias current μ to be 4 for the following simulations in Sections 3.2 and 3.3.

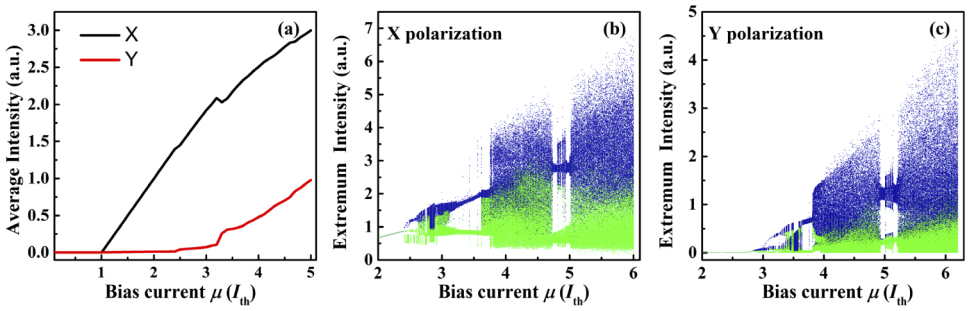

Fig. 2. (a) Average output intensity of *X* mode (black line) and *Y* mode (red line) as a function of bias current μ; (b) Bifurcation diagram of *X* polarization output intensity versus the bias current μ. (c) Bifurcation diagram of *Y* polarization output intensity versus the bias current μ. In (b) and (c), the blue dots and the green dots are top and bottom extrema, respectively.

3.2. Polarization chaos synchronization induced by parallel optical injection

Next, we investigate the property of the polarization chaos synchronization induced by parallel optical injection. In this scenario, the same polarized light emitted by the two VCSELs will be transmitted through the same channel as illustrated in Fig. 1(a).

Figure 3 shows a typical example of chaos synchronization under parallel injection without any parameter mismatch. In this case, $\Delta f = 0$ GHz, $k_{inj} = 80$ ns^{-1}, and other parameter values are the same as that mentioned before. Figure 3(a) presents the chaotic time series outputted by VCSEL1 and VCSEL 2 for the *X* polarization mode, while Fig. 3(b) are the associated temporal waveform for the *Y* polarization mode. Note, all the time series for VCSEL2 are shifted by −7

Optics EXPRESS

mW with respect to the time series of VCSEL1. One can observe that the temporal waveforms from VCSEL1 and VCSEL2 are highly correlated in both the X or Y polarization. Quantitatively, we further calculate the cross-correlation function [Fig. 3(c)] and the synchronization diagram [Fig. 3(d)] for the X polarization mode. From them, we confirm that the chaotic outputs of VCSEL1 and VCSEL2 are well synchronized with a high correlation coefficient $C(\tau) = 0.9994$ around zero time-shift. In particular, we emphasize that the cross-correlation function and the synchronization diagram for the Y polarization mode are similar with Figs. 3(c) and 3(d), so only the results for the X polarization mode are given here.

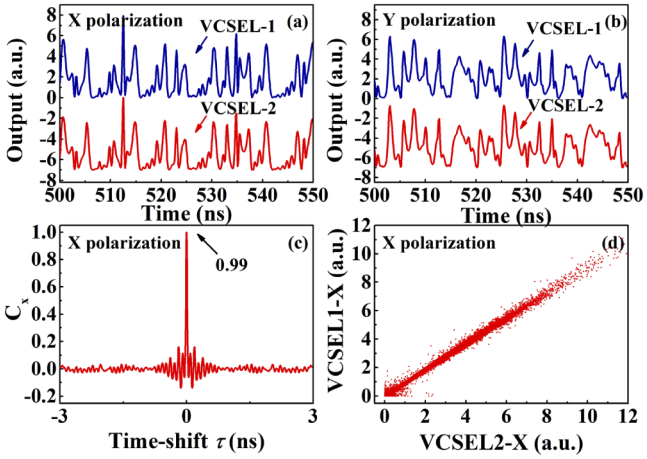

Fig. 3. (a) Time series of VCSEL1 (blue) and VCSEL2 (red) for the X polarization mode; (b) Time series of VCSEL1 (blue) and VCSEL2 (red) for the Y polarization mode; (c) Cross-correlation function and (d) Synchronization diagram between the two X-polarization time series.

For practical VCSELs, device parameters including external parameters and internal parameters cannot be precisely matched. Among the external parameters, the frequency detuning Δf, bias current μ, and coupling coefficient k_{inj} play crucial roles in determining the quality of chaos synchronization. Figure 4 shows the synchronization quality [i.e., maximum cross-correlation coefficient $C(\tau)$] for the X polarization mode and Y polarization mode, calculated in the frequency detuning Δf and coupling coefficient k_{inj} space under the condition of zero delay $\tau = 0$. The synchronization regions for both modes show a similar "V"-shaped symmetry centered on the vertical direction of $\Delta f = 0$ GHz. This means that the frequency detuning Δf plays a vital role in synchronization region, which occurs when the detuning is small. At the same time, a larger coupling coefficient is required to keep a high-quality synchronization with the increase in the positive frequency detuning Δf or negative frequency detuning -Δf. Specifically, it can be seen from Figs. 4(a) and 4(b) that $C(\tau) > 0.9$ appear when k_{inj} is larger than about 20 ns^{-1}. In the range for -10 GHz $< \Delta f <$ 10 GHz and $k_{inj} >$ 20 ns^{-1}, high-quality chaos synchronization can be easier to be obtained. On the other hand, one can find by comparing Figs. 4(a) and 4(b) that at the same frequency detuning Δf, the cross-correlation coefficient for X polarization is larger than that for Y polarization. For instance, in the case $\Delta f = -30$ GHz and $k_{inj} = 50$ ns^{-1}, $C(\tau)$ is about 0.4053 for the X polarization mode but 0.3211 for the Y polarization mode. The reason for this is that the X polarization mode is relatively stronger than the Y polarization mode, which is consistent with the P-I characteristics [Fig. 2(a)].

Figure 5 illustrates the synchronization quality for the X polarization mode and Y polarization mode, calculated in the current deviation $\Delta\mu$ and coupling coefficient k_{inj} space under the condition of $\Delta f = 0$ GHz. In this simulation, the bias current of VCSEL1 is fixed at $\mu = 4$, and

Optics EXPRESS

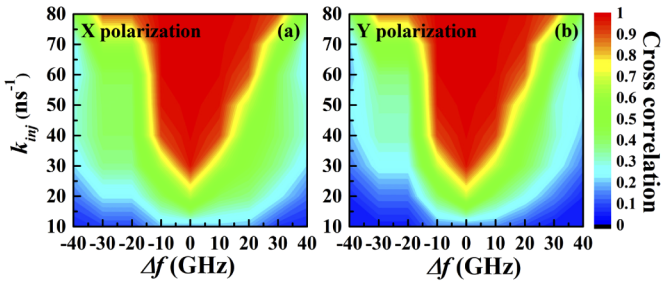

Fig. 4. Cross-correlation graph of frequency detuning Δf (when $\tau = 0$ ps) with respect to the coupling coefficient (k_{inj}). X polarization (a) and Y polarization (b).

only the bias current of VCSEL2 changes with a deviation $\Delta\mu$. From Figs. 5(a) and 5(b), one can observe that the synchronization area for both X and Y polarization modes seems symmetrical about the vertical direction of $\Delta\mu = 0$. Meanwhile, the allowable current mismatch range expands as the coupling coefficient k_{inj} increases. Quantitatively, high-quality chaos synchronization region with a correlation coefficient $C(\tau) > 0.9$ can be obtained in the range of 17.5 ns^{-1} $< k_{inj} <$ 35 ns^{-1} and $-20\% < \Delta\mu < 20\%$.

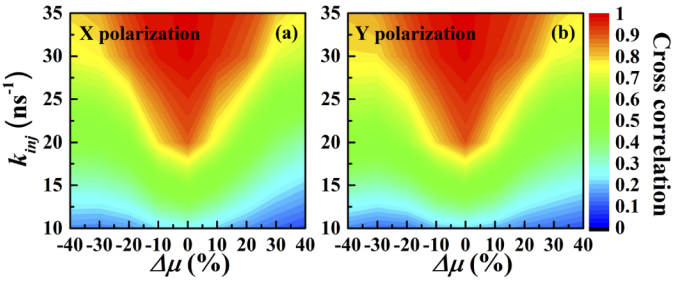

Fig. 5. Cross-correlation graph of the bias current mismatch $\Delta\mu$ (when $\tau = 0$ ps) with respect to the coupling coefficient (k_{inj}). X polarization (a) and Y polarization (b).

Furthermore, we investigate the effect of internal parameter mismatch on the robustness of the X and Y polarization chaos synchronization by means of the synchronization error σ_{error}. Specifically, the internal parameters contain the linewidth enhancement factor α, spin-flip relaxation rate γ_s, field decay rate κ, carrier decay rate γ_N, birefringence γ_p, and dichroism γ_a. In the simulation, VCSEL1 parameters are fixed, while only the internal parameters of VCSEL2 are changed. Moreover, we assume that when one parameter is considered mismatched, the other parameters are completely matched. Figure 6 shows typical results for X polarization [Fig. 6(a)] and Y polarization [Fig. 6(b)] in the synchronization area satisfying $C(\tau) > 0.99$ where $\Delta f = 0$ GHz, $k_{inj} = 80$ ns^{-1}, and $\Delta\mu = 0$. When the error is less than 0.1 (the dotted line in Fig. 6), it is considered to satisfy meet the requirements of information transmission based on chaos synchronization. Generally speaking, the evolution diagram exhibits asymmetries between the positive and negative mismatch for both X polarization and Y polarization. Moreover, negative mismatches are more likely to prevent synchronization than positive parameter mismatches. Specifically, in the case for X polarization [Fig. 6(a)], the field attenuation rate κ has a particularly important influence on the synchronization error, which determines the boundary value of the parameter mismatch. The system will lose synchronization with increased mismatch of the linewidth enhancement factor α and the carrier attenuation rate γ_N. From Fig. 6(a), one can finally obtain an available parameter mismatch range from -10% to 15% to ensure the information

Optics EXPRESS

transmission. In the case of Y polarization [Fig. 6(b)], the linewidth enhancement factor α is the first parameter to prevent synchronization in the positive direction ($\Delta\alpha = 12\%$). The other mismatched parameters in the Y polarization show a similar trend with that in the X polarization: field decay rate κ, linewidth enhancement factor α and carrier decay rate γ_N have great influence on synchronization, while the mismatch of spin flip relaxation rate γ_s, birefringence γ_p, and dichroism γ_a have almost no effect on synchronization within ±20%. In addition, it is apparent from Fig. 6(b) that the Y polarization synchronization is robust within a parameter mismatch of ±12%. All the results show that the internal parameters for chaos synchronization induced by parallel optical injection can be selected in a wide range with some robustness. To our known, this result can be competitive with that in recent works about the chaotic synchronization in mutually coupled semiconductor lasers like in Ref. [30].

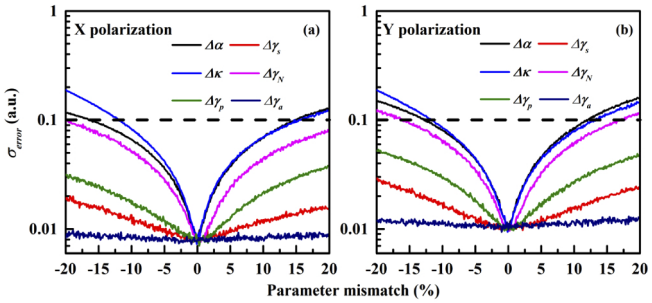

Fig. 6. Evolution diagram of synchronization error (σ_{error}) with internal parameter mismatch in the case of $k_{inj} = 80\,\text{ns}^{-1}$ and $\mu = 4$. (a) X polarization and (b) Y polarization. Note, α: linewidth enhancement factor; γ_s: spin-flip relaxation rate; κ: field decay rate; γ_N: carrier decay rate; γ_p: birefringence; γ_a: dichroism. The horizontal dotted line in plot (a) and (b) represents the synchronization error threshold of 0.1, beyond which the system is considered to be out of synchronization.

3.3. *Polarization chaos synchronization induced by orthogonal optical injection*

In this section, our attention will be focused on the characteristics of the polarization chaos synchronization induced by orthogonal optical injection. In this scenario, the light with the same polarization direction emitted by the two VCSELs is transmitted through two different channels as shown in Fig. 1(b).

Similar to the previous analysis in Section B, we firstly investigate the effect of external parameters on the polarization chaos synchronization. Figure 7 shows the associated synchronization quality [i.e., maximum cross-correlation coefficient $C(\tau)$] calculated in the frequency detuning Δf and coupling coefficient k_{inj} space. In Fig. 7(a) shows the cross-correlation coefficient map between the X polarization light from the VCSEL1 and the Y polarization light from the VCSEL2, while Fig. 7(b) shows the corresponding map between the Y polarization light from the VCSEL1 and the X polarization light from the VCSEL2. Similar to that in the scenario of parallel injection, one can find that the maximum cross-correlation coefficient is also symmetrical along the axis of $\Delta f = 0$ GHz. Synchronization can be observed in the frequency detuning range of -30 GHz ~ 30 GHz. Compared with the case of parallel injection, a larger coupling coefficient is needed to achieve high-quality chaotic synchronization in orthogonal optical injection. Quantitatively, the high-quality synchronization of $C(\tau) > 0.9$ occurs when k_{inj} is bigger than 200 ns^{-1}. In addition, the synchronization area contracts after $k_{inj} > 350\ \text{ns}^{-1}$, and the allowed frequency detuning becomes narrow. Finally, high-quality synchronization under orthogonal injection forms only at the range of $\Delta f = -30 \sim 30$ GHz and $k_{inj} = 200 \sim 400\ \text{ns}^{-1}$, where the maximum cross-correlation coefficient $C(\tau)$ is calculated to be 0.9596. In addition, we want to emphasize that there is a

Optics EXPRESS

relationship between the coupling coefficient (k_{inj}) and the coupling strength (r_{inj}): $k_{inj} = r_{inj}/\tau_{in}$, where τ_{in} is the round-trip time of the laser internal cavity. Generally, commercial VCSELs have an internal cavity length of less than 100 μm. Thus, when the coupling coefficient k_{inj} is equal to 250 ns^{-1}, the corresponding coupling strength r_{inj} can be calculated to be less than 0.56. Similarly, when k_{inj} is equivalent to 400 ns^{-1}, $r_{inj} = 0.89$ can be obtained. In our simulation, the coupling coefficient k_{inj} for a good synchronization under orthogonal injection therefore can meet the current experimental requirements.

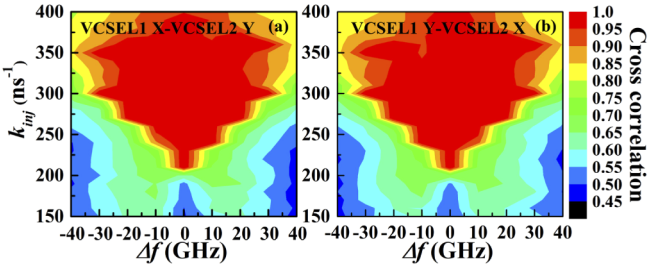

Fig. 7. Cross-correlation graph of frequency detuning Δf (when $\tau = 0$ ps) with respect to the coupling coefficient (k_{inj}). (a) X polarization of VCSEL1 versus Y polarization of VCSEL2; (b) Y polarization of VCSEL1 versus X polarization of VCSEL2.

Figure 8 illustrates the synchronization quality calculated in the current deviation $\Delta\mu$ and coupling coefficient k_{inj} space under the condition of $\Delta f = 0$ GHz. Figure 8(a) shows the cross-correlation coefficient map between the X polarization light from the VCSEL1 and the Y polarization light from the VCSEL2, while Fig. 8(b) shows the corresponding map between the Y polarization light from the VCSEL1 and the X polarization light from the VCSEL2. In this simulation, the bias current of VCSEL1 is also fixed at $\mu = 4$, and only the bias current of VCSEL2 changes with a deviation $\Delta\mu$. It can be seen that chaotic synchronization [$C(\tau)$ > 0.9] is maintained within the region between 200 $ns^{-1} < k_{inj} <$400 ns^{-1} and $-20\% < \Delta\mu <$ 40%. In contrast to parallel injection, this parameter mismatch in orthogonal optical injection is asymmetrical from the cross-correlation graph: a negative mismatch is more likely to prevent the synchronization than a positive mismatch. This means that in a fixed frequency detuning range, a high coupling coefficient value can increase the tolerance of current mismatch.

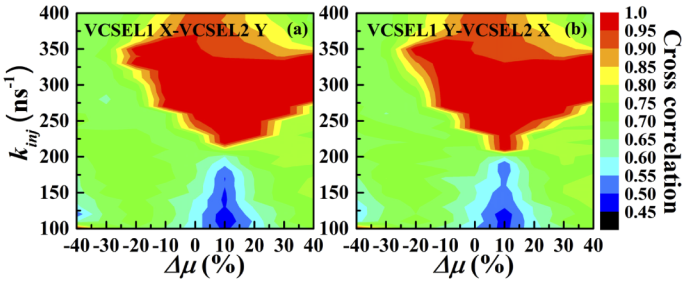

Fig. 8. Cross-correlation graph of the bias current mismatch $\Delta\mu$ (when $\tau = 0$ ps) with respect to the coupling coefficient (k_{inj}). (a) X polarization of VCSEL1 versus Y polarization of VCSEL2; (b) Y polarization of VCSEL1 versus X polarization of VCSEL2.

Now we consider the influence of internal parameter mismatch on chaotic synchronization as shown in Fig. 9. Here, the external parameters are $\Delta f = 0$ GHz, $k_{inj} = 300$ ns^{-1}, and $\Delta\mu = 0$, while only the internal parameters of VCSEL2 are changed. From Fig. 9(a), we find that the synchronization error σ_{error} between the X polarization light of the VCSEL1 and the Y

Optics EXPRESS

polarization light of the VCSEL2 will exceed the guard line of $\sigma_{\text{error}} = 0.1$ [the dotted line in Fig. 9], when the mismatch of the field decay rate κ, the linewidth enhancement factor α and the carrier attenuation rate γ_N are outside the range of −5% to 3%. However, the other three parameters (i.e., the spin flip relaxation rate γ_s, birefringence γ_p, and dichroism γ_a) will almost not affect the synchronization quality. Figure 9(b) characterizes the synchronization error σ_{error} between the Y polarization light from the VCSEL1 and the X polarization light from the VCSEL2. The laser is not affected by $\Delta\gamma_s$, $\Delta\gamma_p$, and $\Delta\gamma_a$, but will lose synchronization when the parameter mismatch of α, κ, and γ_N are greater than 3% along the positive direction. The first loss of synchronization occurs when the mismatch of the carrier attenuation rate $\Delta\gamma_N$ is less than about −3%. And the laser will gradually lose synchronization with increase of the mismatch range of κ and α. In particular, we notice that in contrast with Fig. 6, the synchronization error oscillates obviously with the parameter mismatch varying. This means that the synchronization quality is sensitive to the parameter mismatch under orthogonal injection. The results show that the robustness of the internal parameters that cause chaos under orthogonal injection is within ±3%, which is lower than that in the scenario of parallel injection.

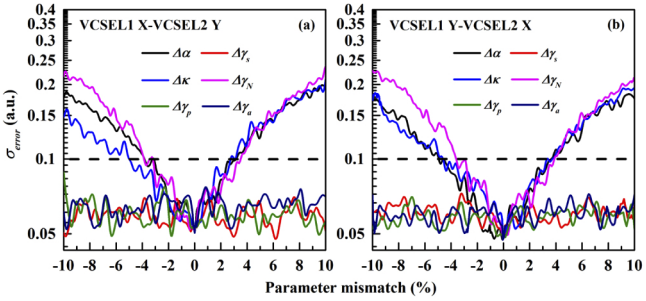

Fig. 9. Evolution diagram of synchronization error (σ_{error}) with internal parameter mismatch in the case of $k_{inj} = 300\,\text{ns}^{-1}$ and $\mu = 4$. (a) X polarization of VCSEL1 versus Y polarization of VCSEL2; (b) Y polarization of VCSEL1 versus X polarization of VCSEL2. Note, α: linewidth enhancement factor; γ_s: spin-flip relaxation rate; κ: field decay rate; γ_N: carrier decay rate; γ_p: birefringence; γ_a: dichroism. The horizontal dotted line in plot (a) and (b) represents the synchronization error threshold of 0.1, beyond which the system is considered to be out of synchronization.

4. Conclusions

We theoretically demonstrate that polarization chaos generated from two free-running VCSELs can be synchronized in a mutually coupled configuration. In detail, we investigate the synchronization quality and robustness of polarization chaos under two scenarios: parallel injection and orthogonal injection. Through analyzing the effect of the external and internal parameters of VCSELs, we confirm that the maximum cross-correlation coefficient can reach 0.9994 in the case of parallel injection and 0.9596 in the case of orthogonal injection, respectively. Further results show that for the parallel injection, its tolerance of the parameter mismatch is ±12% in the range of $-10\,\text{GHz} < \Delta f < 10\,\text{GHz}$ and $k_{inj} > 20\,\text{ns}^{-1}$. For the orthogonal injection, only ±3% parameter mismatch can be tolerated in the range of $-30\,\text{GHz} < \Delta f < 30\,\text{GHz}$ and $200\,\text{ns}^{-1} < k_{inj} < 400\,\text{ns}^{-1}$. Considering that polarization chaos do not require to conceal the time-delay signature in conventional optical feedback schemes, the demonstrated mutually coupled chaos synchronization could be very useful for chaos communication systems and may motivate further related studies.

Funding. National Natural Science Foundation of China (61775158, 61805168, 61961136002, 61927811, U19A2076, 11904057); Program for Guangdong Introducing Innovative and Entrepreneurial Teams; National Crypto Development Foundation (MMJJ20170127); China Postdoctoral Science Foundation (2018M630283, 2019T120197); Natural Science

Optics EXPRESS

Foundation of Shanxi Province (201901D211116, 201801D121015); Program for the Top Young Academic Leaders of High Learning Institutions of Shanxi; Shanxi "1331 Project" Key Innovative Research Team.

Disclosures. The authors declare no conflicts of interest.

Data availability. Data underlying the results presented in this paper are not publicly available at this time but may be obtained from the authors upon reasonable request.

References

1. C. R. Mirasso, P. Colet, and P. García-Fernández, "Synchronization of chaotic semiconductor lasers: Application to encoded communications," IEEE Photon. Technol. Lett **8**(2), 299–301 (1996).
2. G. D. VanWiggeren and R. Roy, "Communications with chaotic lasers," Science **279**(5354), 1198–1200 (1998).
3. J. Goedgebuer, L. Larger, and H. Porte, "Optical cryptosystem based on synchronization of hyperchaos generated by a delayed feedback tunable laser diode," Phys. Rev. Lett. **80**(10), 2249–2252 (1998).
4. J. X. Ke, L. L. Yi, Y. Zhao, Y. P. Yang, Q. B. Zhu-Ge, Y. P. Chen, and W. S. Hu, "32 Gb/s chaotic optical communications by deep-learning-based chaos synchronization," Opt. Lett. **44**(23), 5776–5779 (2019).
5. A. K. Zhao, N. Jiang, S. Q. Liu, Y. Q. Zhang, and K. Qiu, "Generation of synchronized wideband complex signals and its application in secure optical communication," Opt. Express **28**(16), 23363–23373 (2020).
6. A. Argyris, D. Syvridis, L. Larger, V. Annovazzi-Lodi, P. Colet, I. Fischer, J. García-Ojalvo, C. R. Mirasso, L. Pesquera, and K. A. Shore, ", "Chaos-based communications at high bit rates using commercial fibre-optic links."," Nature **438**(7066), 343–346 (2005).
7. L. Roman, M. Jacquot, and L. Larger, "Nonlocal nonlinear electro-optic phase dynamics demonstrating 10 Gb/s chaos communications," IEEE J. Quantum Electron. **46**(10), 1430–1435 (2010).
8. J. X. Ke, L. L. Yi, G. Q. Xia, and W. S. Hu, "Chaotic optical communications over 100-km fiber transmission at 30-Gb/s bit rate," Opt. Lett. **43**(6), 1323–1326 (2018).
9. L. Keuninckx, M. C. Soriano, I. Fischer, C. R. Mirasso, R. M. Nguimdo, and G. V. Sande, "Encryption key distribution via chaos synchronization," Sci. Rep. **7**(1), 43428 (2017).
10. F. Böhm, S. Sahakian, A. Dooms, G. Verschaffelt, and G. V. Sande, "Stable High-Speed Encryption Key Distribution via Synchronization of Chaotic Optoelectronic Oscillators," Phys. Rev. A **13**(6), 064014 (2020).
11. X. F. Li, W. Pan, B. Luo, and D. Ma, "Mismatch robustness and security of chaotic optical communications based on injection-locking chaos synchronization," IEEE J. Quantum Electron. **42**(9), 953–960 (2006).
12. N. Jiang, A. K. Zhao, S. Q. Liu, Y. Q. Zhang, J. F. Peng, and K. Qiu, "Injection-locking chaos synchronization and communication in closed-loop semiconductor lasers subject to phase-conjugate feedback," Opt. Express **28**(7), 9477–9486 (2020).
13. Y. H. Hong, M. W. Lee, P. S. Spencer, and K. A. Shore, "Synchronization of chaos in unidirectionally coupled vertical-cavity surface-emitting semiconductor lasers," Opt. Lett. **29**(11), 1215–1217 (2004).
14. I. Gatare, M. Sciamanna, A. Loquet, and K. Panajotov, "Influence of polarization mode competition on the synchronization two unidirectionally coupled vertical-cavity surface-emitting lasers," Opt. Lett. **32**(12), 1629–1631 (2007).
15. J. F. Liao and J. Q. Sun, "Polarization dynamics and chaotic synchronization in unidirectionally coupled VCSELs subjected to optoelectronic feedback," Opt. Commun. **295**, 188–196 (2013).
16. S. Nazhan, Z. Ghassemlooy, and K. Busawon, "Chaos synchronization in vertical-cavity surface-emitting laser based on rotated polarization-preserved optical feedback," Chaos **26**(1), 013109 (2016).
17. A. Englert, W. Kinzel, Y. Aviad, M. Butkovski, I. Reidler, M. Zigzag, I. Kanter, and M. Rosenbluh, "Zero lag synchronization of chaotic systems with time delayed couplings," Phys. Rev. Lett. **104**(11), 114102 (2010).
18. S. Y. Xiang, Y. A. Han, H. N. Wang, A. J. Wen, and Y. Hao, "Zero-lag chaos synchronization properties in a hierarchical tree-type network consisting of mutually coupled semiconductor lasers," Nonlinear Dyn. **99**(4), 2893–2906 (2020).
19. Q. L. Li, Q. Bao, D. W. Chen, S. N. Yang, M. Hu, R. Zeng, H. Chi, and S. Q. Li, "Point-to-multipoint and ring network communication based on chaotic semiconductor lasers with optical feedback," Appl. Opt. **58**(4), 1025–1032 (2019).
20. M. C. Soriano, J. García-Ojalvo, C. R. Mirasso, and I. Fischer, "Complex photonics: Dynamics and applications of delay-coupled semiconductors lasers," Rev. Mod. Phys. **85**(1), 421–470 (2013).
21. M. Virte, K. Panajotov, H. Thienpont, and M. Sciamanna, "Deterministic polarization chaos from a laser diode," Nat. Photonics **7**(1), 60–65 (2013).
22. Y. Lu, W. Zhang, B. Xu, X. Fan, and Z. He, "Directly modulated vcsels with frequency comb injection for parallel communications," J. Lightwave Technol. **39**(5), 1348–1354 (2021).
23. M. Virte, M. Sciamanna, and K. Panajotov, "Synchronization of polarization chaos from a free-running VCSEL," Opt. Lett. **41**(19), 4492–4495 (2016).
24. W. Y. Yang, G. Q. Xia, F. Z. Jiang, E. Jayaprasath, and Z. M. Wu, "Numerical investigations on multi-channel wideband chaotic signal generation by a multi-transverse mode vertical-cavity surface-emitting laser subject to chaotic optical injection," Appl. Opt. **58**(30), 8160–8166 (2019).
25. M. S. Miguel, Q. Feng, and J. V. Moloney, "Light-polarization dynamics in surface-emitting semiconductor lasers," Phys. Rev. A **52**(2), 1728–1739 (1995).

Optics EXPRESS

26. J. Martin-Regalado, F. Prati, M. S. Miguel, and N. B. Abraham, "Polarization properties of vertical-cavity surface-emitting lasers," IEEE J. Quantum Electron. **33**(5), 765–783 (1997).
27. R. Vicente, J. Mulet, and C. R. Mirasso, "Bistable polarization switching in mutually coupled vertical-cavity surface-emitting lasers," Opt. Lett. **31**(7), 996–998 (2006).
28. J. Ohtsubo, "Chaos synchronization and chaotic signal masking in semiconductor lasers with optical feedback," IEEE J. Quantum Electron. **38**(9), 1141–1154 (2002).
29. H. F. Chen and J. M. Liu, "Open-loop chaotic synchronization of injection-locked semiconductor lasers with gigahertz range modulation," IEEE J. Quantum Electron. **36**(1), 27–34 (2000).
30. T. Wu, Q. L. Li, X. B. Bao, and M. Hu, "Time-delay signature concealment in chaotic secure communication system combining optical intensity with phase feedback," Opt. Commun. **475**, 126042 (2020).